

Local stellar kinematics from RAVE data – III. Radial and vertical metallicity gradients based on red clump stars

S. Bilir,^{1*} S. Karaali,^{1†} S. Ak,¹ Ö. Önal,¹ N. D. Dağtekin,¹ T. Yontan,¹ G. Gilmore^{2,3} and G. M. Seabroke⁴

¹*Department of Astronomy and Space Sciences, Science Faculty, Istanbul University, 34119, Istanbul, Turkey*

²*Institute of Astronomy, Madingley Road, Cambridge CB3 0HA*

³*Astronomy Department, Faculty of Science, King Abdulaziz University, PO Box 80203, Jeddah 21589, Saudi Arabia*

⁴*Mullard Space Science Laboratory, University College London, Hombury St Mary, Dorking RH5 6NT*

Accepted 2012 January 13. Received 2012 January 13; in original form 2011 December 12

ABSTRACT

We investigate radial and vertical metallicity gradients for a sample of red clump stars from the RAdial Velocity Experiment (RAVE) Data Release 3. We select a total of 6781 stars, using a selection of colour, surface gravity and uncertainty in the derived space motion, and calculate for each star a probabilistic (kinematic) population assignment to a thin or thick disc using space motion and additionally another (dynamical) assignment using stellar vertical orbital eccentricity. We derive almost equal metallicity gradients as a function of the Galactocentric distance for the high-probability thin-disc stars and for stars with vertical orbital eccentricities consistent with being dynamically young, $e_v \leq 0.07$, i.e. $d[M/H]/dR_m = -0.041 \pm 0.003$ and $d[M/H]/dR_m = -0.041 \pm 0.007$ dex kpc⁻¹. Metallicity gradients as a function of the distance from the Galactic plane for the same populations are steeper, i.e. $d[M/H]/dz_{\max} = -0.109 \pm 0.008$ and $d[M/H]/dz_{\max} = -0.260 \pm 0.031$ dex kpc⁻¹, respectively. R_m and z_{\max} are the arithmetic mean of the perigalactic and apogalactic distances, and the maximum distance to the Galactic plane, respectively. Samples including more thick-disc red clump giant stars show systematically shallower abundance gradients. These findings can be used to distinguish between different formation scenarios of the thick and thin discs.

Key words: stars: abundances – Galaxy: abundances – Galaxy: disc – Galaxy: evolution.

1 INTRODUCTION

Metallicity gradients play an important role in understanding the formation of disc populations of the galaxies. In the Milky Way Galaxy, there is extensive information establishing a radial gradient in young stars and in the interstellar medium (Shaver et al. 1983; Luck, Kovtyukh & Andrievsky 2006; Luck & Lambert 2011). Values typically derived are $d[Fe/H]/dR_G = -0.06 \pm 0.01$ dex kpc⁻¹, within 2–3 kpc of the Sun. Much effort to search for local abundance variations, and abundance variations with azimuth, shows little if any detectable variation in young systems (Luck et al. 2011), showing the interstellar medium to be well mixed on quite large scales, supporting the importance of gas flows.

Extant data suggest vertical metallicity gradients in the $-0.4 < d[M/H]/dz < -0.2$ dex kpc⁻¹ range for relatively small distances

from the Galactic plane, i.e. $z < 4$ kpc (Trefzger, Pel & Gabi 1995; Karaali et al. 2003; Du et al. 2004; Ak et al. 2007a; Peng, Du & Wu 2011). For intermediate z -distances, where the thick disc is dominant, the vertical metallicity gradient is low, $d[M/H]/dz = -0.07$ dex kpc⁻¹, and the radial gradient is only marginal, $-0.02 \leq d[M/H]/dR \leq 0$ dex kpc⁻¹ (Rong, Buser & Karaali 2001). There is some evidence that metallicity gradients for relatively short vertical distances, $z < 2.5$ kpc, show systematic fluctuations with Galactic longitude, similar to those of thick-disc scaleheight, which may be interpreted as a common flare effect of the disc (Bilir et al. 2006, 2008; Ak et al. 2007b; Cabrera-Lavers et al. 2007; Yaz & Karaali 2010).

Quantifying the abundance distribution functions and their radial and vertical gradients in both thin and thick discs can be achieved using stellar abundances, especially those from major surveys such as RAdial Velocity Experiment (RAVE; Steinmetz et al. 2006) and Sloan Digital Sky Survey (SDSS; Abazajian et al. 2003). RAVE is a multifibre spectroscopic astronomical survey in the Milky Way, which covers just over the half of the Southern Hemisphere, using

*E-mail: sbilir@istanbul.edu.tr

†Retired.

the 1.2-m UK Schmidt Telescope of the Australian Astronomical Observatory (Steinmetz et al. 2006; Zwitter et al. 2008; Siebert et al. 2011). RAVE’s primary aim is to derive the radial velocity of stars from the observed spectra for solar neighbourhood stars. Additional information is also derived, such as photometric parallax and stellar atmospheric parameters, i.e. effective temperature, surface gravity, metallicity and elemental abundance data. This information is important in calculating metallicity gradients, which provides data about the formation and evolution of the Galaxy. As the data were obtained from solar neighbourhood stars, we have limitations to distance and range of metallicity. However, the metallicity measurements are of high internal accuracy which is an advantage for our work.

In a recent study carried out by Chen et al. (2011), a vertical metallicity gradient of $-0.22 \text{ dex kpc}^{-1}$ was claimed for the thick disc. They used the SDSS DR8 (Aihara et al. 2011) data set to identify a sample of red horizontal branch (RHB) stars, and for this sample they derived the steepest metallicity gradient for the thick disc currently in the literature. RHB stars are very old, on average, so it is feasible that they can have a different metallicity variation than younger stars. However, the difference between their metallicity gradient and others’ in the literature for the thick disc is large, which motivates confirmation by other works with different data.

In our previous study (Coşkunoğlu et al. 2012, paper II), we investigated the metallicity gradient of a dwarf sample and confirmed the radial metallicity gradient of $-0.04 \text{ dex kpc}^{-1}$ based on calibrated metallicities from the RAVE Data Release 3 (RAVE DR3) (Coşkunoğlu et al. 2012, and the references therein, paper I). Additionally, we showed that the radial metallicity gradient is steeper for our sample which is statistically selected to favour younger stars, i.e. F-type stars with orbital eccentricities $e_v \leq 0.04$, i.e. $d[M/H]/dR_m = -0.051 \pm 0.005 \text{ dex kpc}^{-1}$. Vertical metallicity gradients could not be derived in this study due to short z -distances from the Galactic plane. Therefore, in the present study, we analyse stellar abundance gradients of red clump (RC) stars from RAVE data.

RC stars are core helium-burning stars in an identical evolutionary phase to those which make up the horizontal branch in globular clusters. However, in intermediate- and higher-metallicity systems only the red end of the distribution is seen, forming a clump of stars in the colour–magnitude diagram. In recent years much work has been devoted to studying the suitability of RC stars for application as a distance indicator. Their absolute magnitude in the optical ranges from $M_V = +0.70 \text{ mag}$ for those of spectral type G8 III to $M_V = +1.0 \text{ mag}$ for type K2 III (Keenan & Barnbaum 1999). The absolute magnitude of these stars in the K band is $M_K = -1.61 \pm 0.03 \text{ mag}$ with negligible dependence on metallicity (Alves 2000), but with a real dispersion (see below), and in the I band $M_I = -0.23 \pm 0.03 \text{ mag}$, again without dependence on metallicity (Paczynski & Stanek 1998). RAVE DR3 RC giant stars occupy a relatively larger z -distance interval than do RAVE DR3 dwarfs. Hence, we should have sufficient data to be able to derive abundance gradients for both directions, radial and vertical. As the RHB stars are on the extended branch of RC stars, we anticipate the results to be similar to the RHB stars claimed in Chen et al. (2011), and so are able to test their result.

The structure of the paper is as follows. Data selection is described in Section 2; calculated space velocities and orbits of sample stars are described in Section 3. Population analysis and results are given in Section 4 and 5, respectively. Finally, a discussion and conclusion are presented in Section 6.

2 DATA

The data were selected from the RAVE DR3 (Siebert et al. 2011). The RAVE DR3 reports 83 072 radial velocity measurements for stars $9 \leq I \leq 12 \text{ mag}$. This release also provides stellar atmospheric parameters for 41 672 spectra representing 39 833 individual stars (Siebert et al. 2011). The accuracy of the radial velocities is high, marginally improved with DR3: the distribution of internal errors in radial velocities has a mode of 0.8 km s^{-1} and a median of 1.2 km s^{-1} , while 95 per cent of the sample has an internal error smaller than 5 km s^{-1} . The uncertainties for the stellar atmospheric parameters are typically 250 K for the effective temperature T_{eff} , 0.43 dex for the surface gravity $\log g$ and 0.2 dex for $[M/H]$. While RAVE supports a variety of chemical abundance scales, we use here just the public DR3 values. Since anticipated gradients are small, this provides a well-defined set of parameters for analysis. The proper motions of the stars were taken from RAVE DR3 values, which were compiled from PPMX, *Tycho-2*, SSS and UCAC2 catalogues. The distribution of RAVE DR3 stars in the Equatorial and Galactic coordinate planes are shown in Fig. 1.

We applied the following constraints to obtain a homogeneous RC sample with best quality: (i) $2 \leq \log g (\text{cm s}^{-2}) \leq 3$ (Puzeras et al. 2010), (ii) the Two Micron All Sky Survey (2MASS; Skrutskie et al. 2006) photometric data are of quality labelled as ‘AAA’ and (iii) $(J - H)_0 > 0.4$ (Bilir et al. 2011). The numerical values for χ^2 and the median of the S/N value of sample spectra (totally 7985 stars) thus obtained are 671 and 41, respectively. Proper motions for 139 out of the 7985 stars are not available in the RAVE DR3; hence, these values are provided from the PPMXL catalogue of Roeser, Demleitner & Schilbach (2010). Distances were obtained by combining the apparent K_s magnitude of the star in query and

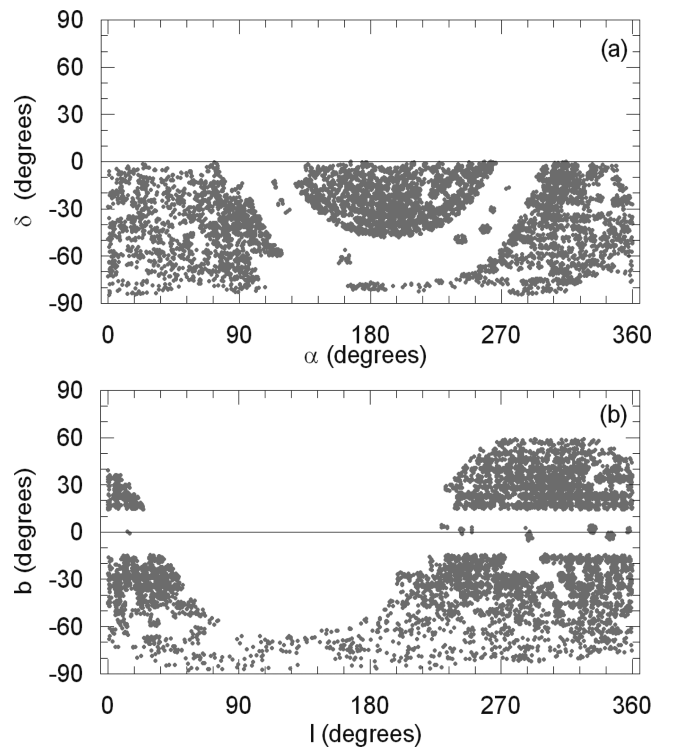


Figure 1. Distribution of RAVE DR3 stars in the Equatorial (top) and Galactic (bottom) coordinate planes.

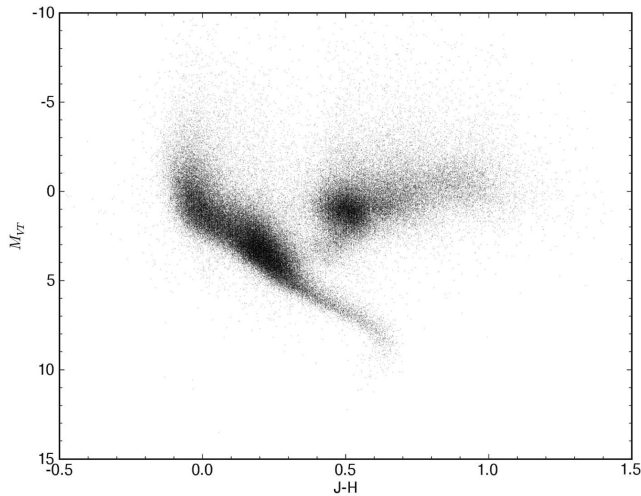


Figure 2. The colour–absolute magnitude diagram for the revised *Hipparcos* catalogue (van Leeuwen 2007) cross-matched with 2MASS (Cutri et al. 2003). The very well illustrated RC justifies the colour selection used in our study.

the absolute magnitude $M_{K_s} = -1.54 \pm 0.04$ mag, adopted for all RC stars (Groenewegen 2008), whereas the $E(B - V)$ reddening was obtained iteratively by using published methodology (for more detailed information regarding the iterations see Coşkunoğlu et al. 2011, and the references therein). Then, the de-reddening of magnitudes and colours in 2MASS was carried out by the following equations with the coefficient of Fiorucci & Munari (2003):

$$\begin{aligned} J_o &= J - 0.887 \times E(B - V) \\ (J - H)_o &= (J - H) - 0.322 \times E(B - V) \\ (H - K_s)_o &= (H - K_s) - 0.183 \times E(B - V). \end{aligned} \quad (1)$$

Note the real dispersion in absolute magnitude among RC stars (Fig. 2). This will have the effect of blurring the derived distances and so smoothing any derived gradient. Given that we search for a linear gradient, such distance uncertainties will tend to somewhat reduce any measured gradient. Given our results below, we consider any such effect to be second order.

The distance range of the sample and the median of the distances are $0.2 \leq d \leq 3.4$ and 1.34 kpc, respectively (Fig. 3), which are sufficient to investigate both radial and vertical metallicity gradients. The distribution of colour excess $E(B - V)$ is given in three categories, i.e. $0^\circ < |b| \leq 30^\circ$, $30^\circ < |b| \leq 60^\circ$ and $60^\circ < |b| \leq 90^\circ$, whose mean values are 0.14, 0.06 and 0.02 mag, respectively (Fig. 4). The reddening is rather small at intermediate and high Galactic latitudes, as expected. The projection of the sample stars on to the (X, Y) and (X, Z) planes (Fig. 5) shows that their distribution is biased (by design: RAVE does not observe towards the Galactic bulge and so); the medians of the heliocentric coordinates are $X = 0.52$, $Y = -0.59$, $Z = -0.41$ kpc.

3 SPACE VELOCITIES AND ORBITS

We combined the distances estimated in Section 2 with RAVE kinematics and the available proper motions, applying the algorithms and the transformation matrices of Johnson & Soderblom (1987) to obtain their Galactic space velocity components (U, V, W). In the calculations epoch J2000 was adopted as described in the International Celestial Reference System of the *Hipparcos* and *Tycho-2*

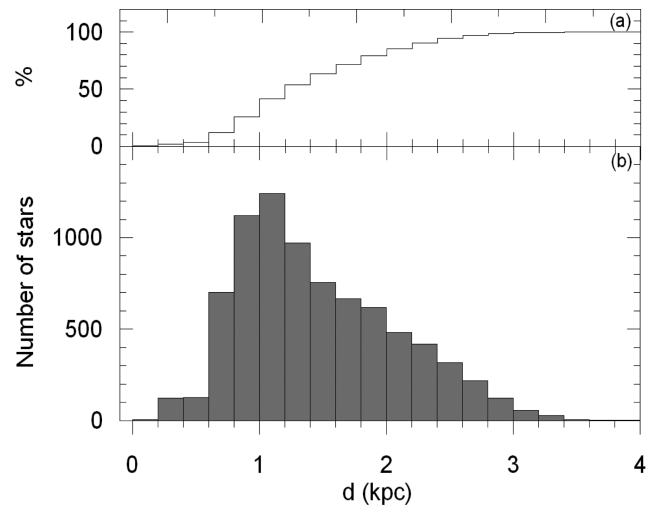


Figure 3. Cumulative (panel a) and frequency (panel b) distributions of distances of our sample of RAVE RC giants.

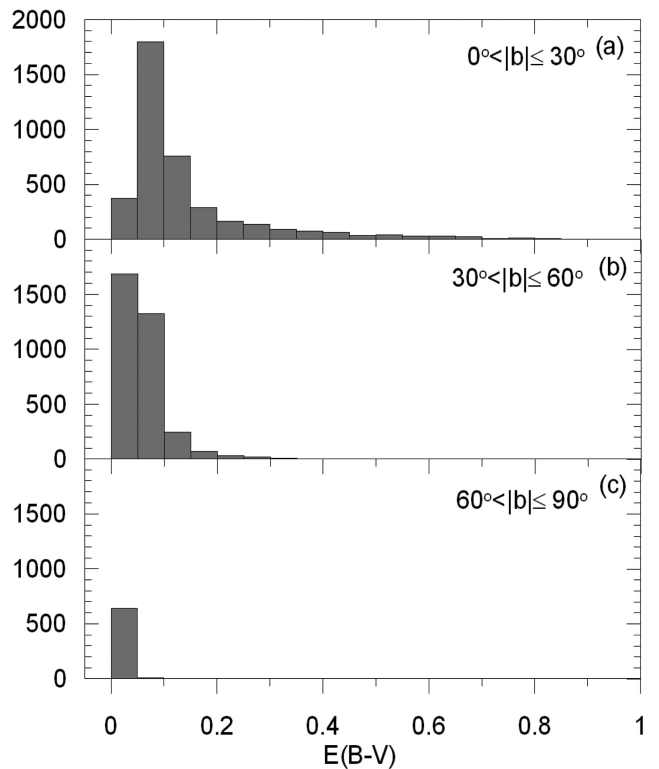


Figure 4. Distribution of colour excess $E(B - V)$ for our sample of RAVE RC giants.

catalogues (ESA 1997). The transformation matrices use the notation of a right-handed system. Hence, U, V and W are the components of a velocity vector of a star with respect to the Sun, where U is positive towards the Galactic Centre ($l = 0^\circ, b = 0^\circ$), V is positive in the direction of Galactic rotation ($l = 90^\circ, b = 0^\circ$) and W is positive towards the North Galactic Pole ($b = 90^\circ$).

We adopted the value of the rotation speed of the Sun as 222.5 km s^{-1} . Correction for differential Galactic rotation is necessary for accurate determination of the U, V and W velocity components. The effect is proportional to the projection of the distance

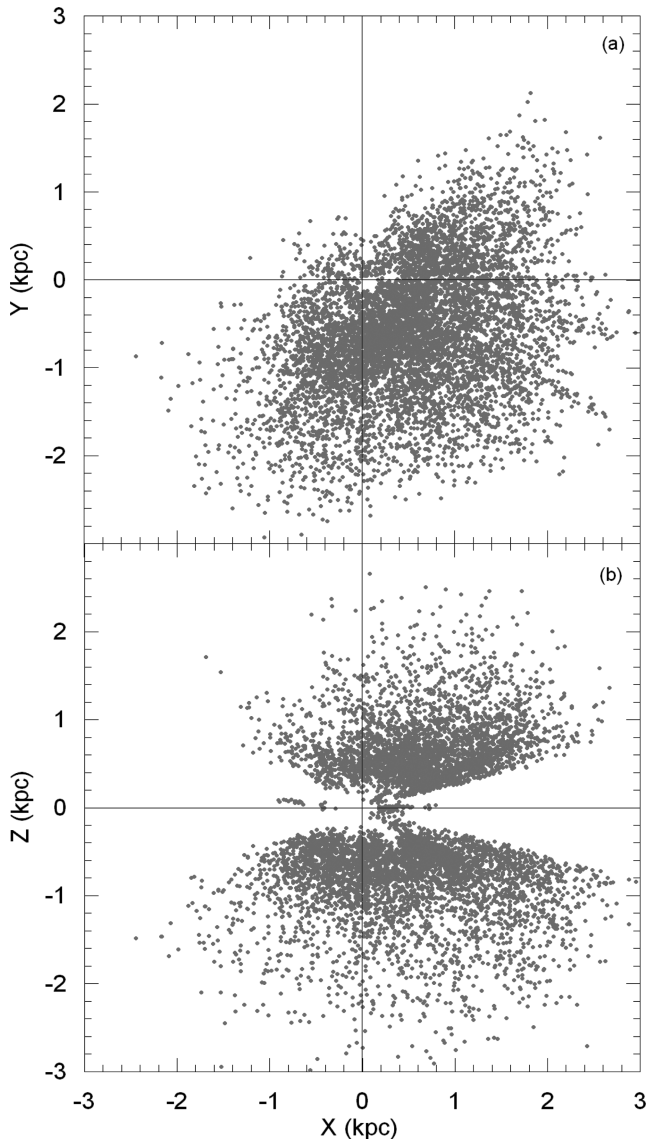


Figure 5. Space distributions of our sample of RAVE RC giants projected on to two Galactic planes: (a) X - Y and (b) X - Z .

to the stars on to the Galactic plane, i.e. the W velocity component is not affected by Galactic differential rotation (Mihalas & Binney 1981). We applied the procedure of Mihalas & Binney (1981) to the distribution of the sample stars and estimated the first-order Galactic differential rotation corrections for the U and V velocity components of the sample stars. The range of these corrections is $-92 < dU < 58$ and $6 < dV < 7 \text{ km s}^{-1}$ for U and V , respectively. As expected, U is affected more than the V component. Also, the high values for the U component show that corrections for differential Galactic rotation cannot be ignored. One notes that Galactic differential rotation corrections are rather larger than the corresponding ones for dwarfs (Coşkunoğlu et al. 2011). The U , V and W velocities were reduced to local standard of rest (LSR) by adopting the solar LSR velocities in Coşkunoğlu et al. (2011), i.e. $(U_{\odot}, V_{\odot}, W_{\odot}) = (8.83, 14.19, 6.57) \text{ km s}^{-1}$.

The uncertainties of the space velocity components U_{err} , V_{err} and W_{err} were computed by propagating the uncertainties of the proper motions, distances and radial velocities, again using an algorithm

by Johnson & Soderblom (1987). Then, the error for the total space motion of a star follows from the equation

$$S_{\text{err}}^2 = U_{\text{err}}^2 + V_{\text{err}}^2 + W_{\text{err}}^2. \quad (2)$$

The mean S_{err} and standard deviation (s) for space velocity errors are $S_{\text{err}} = 39$ and $s = 36 \text{ km s}^{-1}$, respectively. We now remove the most discrepant data from the analysis, knowing that outliers in a survey such as this will preferentially include stars which are systematically misanalysed binaries, etc. Astrophysical parameters for such stars are also likely to be relatively unreliable. Thus, we omit stars with errors that deviate by more than the sum of the standard error and the standard deviation, i.e. $S_{\text{err}} > 75 \text{ km s}^{-1}$. This removes 1204 stars, ~ 15.1 per cent of the sample. Thus, our sample was reduced to 6781 stars, those with more robust space velocity components. After applying this constraint, the mean values and the standard deviations for the velocity components were reduced to $(U_{\text{err}}, V_{\text{err}}, W_{\text{err}}) = (15.03 \pm 10.61, 15.12 \pm 11.20, 15.68 \pm 12.06) \text{ km s}^{-1}$. The distribution of the errors for the space velocity components is given in Fig. 6. In this study, we used only the subsample of stars (6781 stars) with standard error $S_{\text{err}} \leq 75 \text{ km s}^{-1}$. The U , V , W velocity diagrams for these stars are shown in Fig. 7. The centre of the distributions deviates from the zero-points of the U , V and W velocity components, further indicating the need for an LSR reduction.

To complement the chemical abundance data, accurate kinematic data have been obtained and used to calculate individual Galactic orbital parameters for all stars. The shape of the stellar orbit is a proxy, through the age-velocity dispersion relation, for age, with more circular orbits hosting statistically younger stars.

In order to calculate those parameters we used standard gravitational potentials well described in the literature (Miyamoto & Nagai 1975; Hernquist 1990; Johnston, Spergel & Hernquist 1995; Dinescu, Girard & van Altena 1999) to estimate orbital elements of each of the sample stars. The orbital elements for a star used in our work are the mean of the corresponding orbital elements calculated over 15 orbital periods of that specific star. The orbital integration typically corresponds to 3 Gyr and is sufficient to evaluate the orbital elements of solar neighbourhood stars, most of which have orbital periods below 250 Myr.

Solar neighbourhood velocity space includes well-established substructures that resemble classic moving groups or stellar streams (Dehnen 1998; Skuljan, Hearnshaw & Cottrell 1999; Nordström et al. 2004). Famaey et al. (2005), Famaey, Siebert & Jorissen (2008) and Pompéia et al. (2011) show that, although these streams include clusters, after which they are named, and evaporated remnants from these clusters, the majority of stars in these streams are not coeval but include stars of different ages, not necessarily born in the same place nor at the same time. They argue that these streams are dynamical (resonant) in origin, probably related to dynamical perturbations by transient spiral waves (De Simone, Wu & Tremaine 2004), which migrate stars to specific regions of the UV plane. Stars in a dynamical stream just share a common velocity vector at this particular epoch. These authors further point out the obvious and important point that dynamical streams are kinematically young, and so integrating backwards in a smooth stationary axisymmetric potential the orbits of the stars belonging to these streams are non-physical. RAVE stars are selected to avoid the Galactic plane ($|b| > 10^\circ$). Dynamical perturbations by transient spiral waves are strongest closest to the Galactic plane so there will be fewer dynamical stream stars in our RAVE sample. Hence, contamination of the dynamical stream stars is unlikely to affect our statistical results.

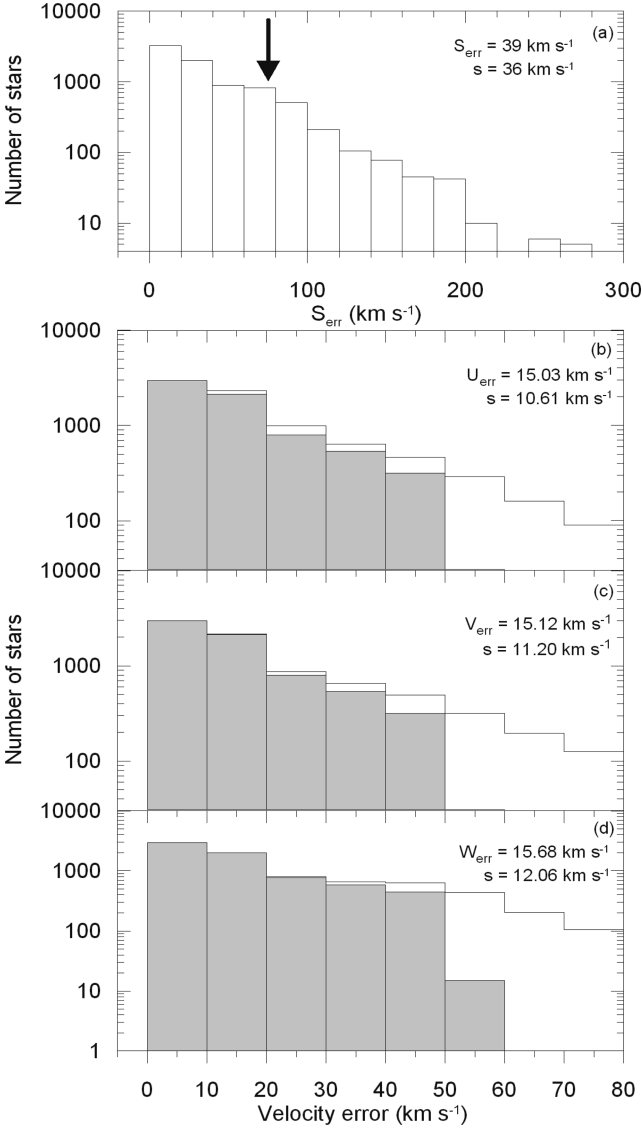


Figure 6. Error histograms for space velocity (panel a) and its components (panels b–d) for our sample of RAVE RC stars. The arrow in panel (a) indicates the upper limit of the total error adopted in this work. The shaded part of the histogram indicates the error for different velocity components of stars after removing the stars with large space velocity errors.

To determine a possible orbit, we first perform test-particle integration in a Milky Way potential which consists of a logarithmic halo of the form

$$\Phi_{\text{halo}}(r) = v_0^2 \ln \left(1 + \frac{r^2}{d^2} \right), \quad (3)$$

with $v_0 = 186 \text{ km s}^{-1}$ and $d = 12 \text{ kpc}$. The disc is represented by a Miyamoto–Nagai potential:

$$\Phi_{\text{disc}}(R, z) = -\frac{GM_d}{\sqrt{R^2 + \left(a_d + \sqrt{z^2 + b_d^2} \right)^2}}, \quad (4)$$

with $M_d = 10^{11} M_{\odot}$, $a_d = 6.5 \text{ kpc}$ and $b_d = 0.26 \text{ kpc}$. Finally, the bulge is modelled as a Hernquist potential,

$$\Phi_{\text{bulge}}(r) = -\frac{GM_b}{r+c}, \quad (5)$$

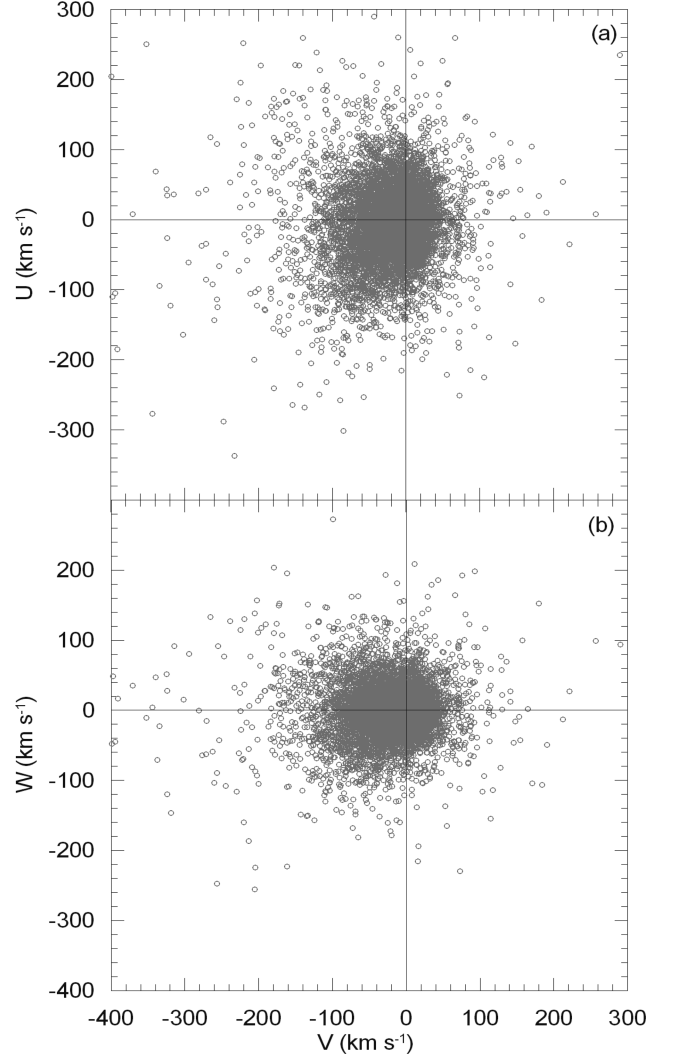


Figure 7. The distribution of velocity components of our final cleaned sample of RAVE RC stars with high-quality data, in two projections: (a) $U - V$ and (b) $W - V$.

using $M_b = 3.4 \times 10^{10} M_{\odot}$ and $c = 0.7 \text{ kpc}$. The superposition of these components gives quite a good representation of the Milky Way. The circular speed at the solar radius is $\sim 220 \text{ km s}^{-1}$. $P_{\text{LSR}} = 2.18 \times 10^8 \text{ yr}$ is the orbital period of the LSR and $V_c = 222.5 \text{ km s}^{-1}$ denotes the circular rotational velocity at the solar Galactocentric distance, $R_0 = 8 \text{ kpc}$.

For our analysis of gradients, we are interested in the mean radial Galactocentric distance (R_m) as a function of the stellar population and the orbital shape. Wilson et al. (2011) have analysed the radial orbital eccentricities of a RAVE sample of thick-disc stars, to test thick-disc formation models. Here we focus on possible local gradients, so we instead consider the *vertical* orbital eccentricity, e_v . R_m is defined as the arithmetic mean of the final perigalactic (R_p) and apogalactic (R_a) distances, and z_{max} and z_{min} are the final maximum and minimum distances, respectively, to the Galactic plane, whereas e_v is defined as follows:

$$e_v = \frac{(|z_{\text{max}}| + |z_{\text{min}}|)}{R_m}, \quad (6)$$

where $R_m = (R_a + R_p)/2$ (Pauli 2005). Due to z -excursions R_p and R_a can vary; however, this variation is not more than 5 per cent.

4 POPULATION ANALYSIS

4.1 Classification using space motions

The procedure of Bensby, Feltzing & Lundström (2003) and Bensby et al. (2005) was used to separate sample stars into different populations. This kinematic methodology assumes that Galactic space velocities for the thin disc (D), thick disc (TD) and stellar halo (H) with respect to the LSR have Gaussian distributions as follows:

$$f(U, V, W) = k \times \exp\left(-\frac{U_{\text{LSR}}^2}{2\sigma_{U_{\text{LSR}}}^2} - \frac{(V_{\text{LSR}} - V_{\text{asym}})^2}{2\sigma_{V_{\text{LSR}}}^2} - \frac{W_{\text{LSR}}^2}{2\sigma_{W_{\text{LSR}}}^2}\right), \quad (7)$$

where

$$k = \frac{1}{(2\pi)^{3/2} \sigma_{U_{\text{LSR}}} \sigma_{V_{\text{LSR}}} \sigma_{W_{\text{LSR}}}} \quad (8)$$

normalizes the expression. For consistency with other analyses $\sigma_{U_{\text{LSR}}}$, $\sigma_{V_{\text{LSR}}}$ and $\sigma_{W_{\text{LSR}}}$ were adopted as the characteristic velocity dispersions: 35, 20 and 16 km s⁻¹ for thin disc (D); 67, 38 and 35 km s⁻¹ for thick disc (TD); and 160, 90 and 90 km s⁻¹ for halo (H), respectively (Bensby et al. 2003). V_{asym} is the asymmetric drift: -15, -46 and -220 km s⁻¹ for thin disc, thick disc and halo, respectively. LSR velocities were taken from Coşkunoğlu et al. (2011) and these values are $(U, V, W)_{\text{LSR}} = (8.83 \pm 0.24, 14.19 \pm 0.34, 6.57 \pm 0.21)$ km s⁻¹.

The probability of a star of being ‘a member’ of a given population with respect to a second population is defined as the ratio of the $f(U, V, W)$ distribution functions times the ratio of the local space densities for two populations. Thus,

$$TD/D = \frac{X_{\text{TD}}}{X_{\text{D}}} \times \frac{f_{\text{TD}}}{f_{\text{D}}} \quad TD/H = \frac{X_{\text{TD}}}{X_{\text{H}}} \times \frac{f_{\text{TD}}}{f_{\text{H}}} \quad (9)$$

are the probabilities for a star being classified as a thick-disc star relative to it being a thin-disc star, and relative to it being a halo star, respectively. X_{D} , X_{TD} and X_{H} are the local space densities for thin disc, thick disc and halo, i.e. 0.94, 0.06 and 0.0015, respectively (Robin et al. 1996; Buser, Rong & Karaali 1999). We followed the

argument of Bensby et al. (2005) and separated the sample stars into four categories: $TD/D \leq 0.1$ (high-probability thin-disc stars), $0.1 < TD/D \leq 1$ (low-probability thin-disc stars), $1 < TD/D \leq 10$ (low-probability thick-disc stars) and $TD/D > 10$ (high-probability thick-disc stars). Fig. 8 shows the $U - V$ and $W - V$ diagrams as a function of population types defined by using the Bensby et al. (2003) criteria. It is evident from Fig. 8 that the kinematic population assignments are strongly affected by space-motion uncertainties. 3385 and 1151 stars of the sample were classified as high- and

Table 1. The space velocity component ranges for the range of population types into which our RAVE RC stars have been classified.

Parameters	U (km s ⁻¹)	V (km s ⁻¹)	W (km s ⁻¹)	N
$TD/D \leq 0.1$	(-98, 97)	(-60, 51)	(-44, 43)	3385
$0.1 < TD/D \leq 1$	(-133, 123)	(-78, 72)	(-57, 58)	1151
$1 < TD/D \leq 10$	(-151, 154)	(-93, 85)	(-69, 69)	646
$TD/D > 10$	(-337, 290)	(-400, 291)	(-344, 273)	1599

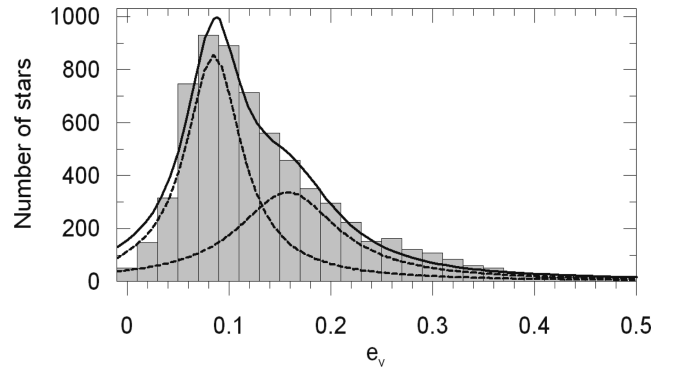


Figure 9. The distribution of the vertical orbital eccentricity for our sample of RC stars. The dashed lines indicate the stars with $e_v \leq 0.12$ (the one with higher mod) and $0.12 < e_v \leq 0.25$ eccentricities (lower mod), respectively, whereas the solid line corresponds to the whole sample.

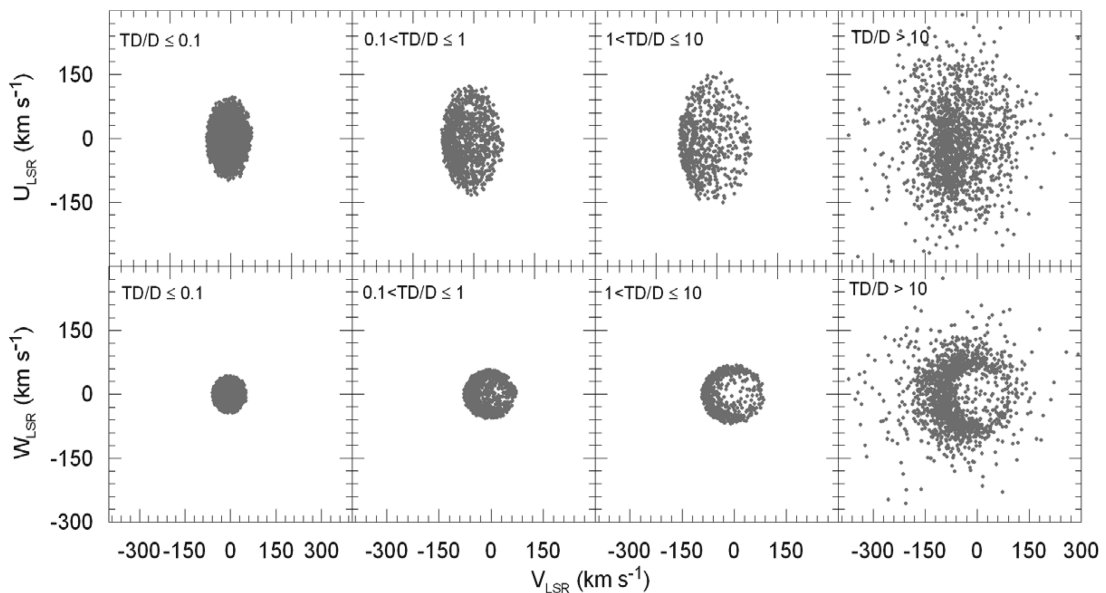


Figure 8. $U - V$ and $W - V$ diagrams for our sample of RC stars, applying the Bensby et al. (2003) population classification criterion. It is apparent that space-motion uncertainties remain significant, even for this sample.

Table 2. Stellar atmospheric parameters, and astrometric, kinematic and dynamic data for the whole sample: (1) our catalogue number, (2) RAVEID, (3, 4) Equatorial coordinates in degrees (J2000), (5) T_{eff} in K, (6) $\log g$ (cm s^{-2}) in dex, (7) calibrated metallicity [M/H] (dex), (8, 9) proper motion components in mas yr^{-1} , (10) d in kpc, (11) heliocentric radial velocity in km s^{-1} , (12–17) Galactic space velocity components, and their respective errors in km s^{-1} , (18–19) perigalactic and apogalactic distance in kpc, (20, 21) minimum and maximum distance from the Galactic plane in kpc, (22) T_{eff}/D ratio as mentioned in the text. $T_{\text{eff}}/D = 999.999$ shows the value of $T_{\text{eff}}/D > 999$.

(1)	(2)	(3)	(4)	(5)	(6)	(7)	(8)	(9)	(10)	(11)	(12)	(13)	(14)	(15)	(16)	(17)	(18)	(19)	(20)	(21)	(22)
ID	Designation	α	δ	T_{eff}	$\log g$	[M/H]	$\mu_{\alpha} \cos \delta$	μ_{δ}	d	γ	U_{LSR}	U_{err}	V_{LSR}	V_{err}	W_{LSR}	W_{err}	d_{per}	d_{apo}	z_{min}	z_{max}	T_{eff}/D
1	J00002.9-490434	0.012 167	-49.076 083	4963	2.99	-0.32	20.2	-11.7	1.920	-25.23	-109.28	20.12	-154.86	21.00	31.23	8.61	1.822	8.580	-2.096	4.316	999.999
2	J000013.7-725608	0.056 875	-72.935 667	4491	2.24	0.01	18.8	-4.0	0.885	10.40	-38.44	13.36	-39.40	11.97	-4.49	10.36	5.433	7.994	-0.627	0.628	0.027
3	J000019.8-283022	0.082 458	-28.505 972	4596	2.14	-0.43	19.2	-9.2	1.243	18.10	-64.75	16.37	-83.65	16.70	-32.70	3.37	3.582	8.415	-1.397	1.398	32.168
4	J000207.7-540333	0.532 167	-54.059 028	4588	2.06	-0.54	15.5	-10.0	1.631	14.53	-50.67	23.08	-110.26	22.61	4.76	11.20	2.790	7.880	-1.444	1.444	359.507
5	J000208.9-843734	0.536 875	-84.626 139	4648	2.21	-0.59	-11.2	2.4	0.901	84.39	106.73	10.02	-18.51	7.93	-37.96	9.05	5.008	10.153	-0.937	0.940	1.708
6	J000211.9-633612	0.549 750	-63.603 389	4698	2.59	-0.48	13.1	-8.3	1.449	61.38	-11.57	22.70	-99.34	22.22	-26.45	15.03	3.129	7.538	-1.253	1.256	66.785
7	J000214.2-083408	0.559 042	-8.568 889	5237	2.80	-0.53	13.2	-2.6	1.199	11.97	-61.50	12.23	-27.10	11.59	-23.51	4.74	5.805	9.049	-1.256	1.253	0.061
8	J000241.8-355010	0.673 958	-35.836 028	4661	2.86	-0.23	22.8	-6.4	1.382	-14.50	-105.23	10.45	-90.62	11.37	-1.53	2.63	3.177	9.171	-1.450	1.450	137.423
9	J000257.3-060701	0.738 542	-6.117 028	4739	2.57	-0.40	29.7	7.5	1.149	1.42	-165.05	17.71	-25.73	16.15	-10.23	7.25	4.457	13.125	-1.446	1.462	30.648
10	J000324.5-821243	0.852 167	-82.212 028	4733	2.60	-0.50	-4.2	-10.5	1.015	45.37	73.12	12.40	-37.92	10.18	24.92	11.39	4.780	8.590	-0.725	0.726	0.193
11	J000324.5-821243	0.852 167	-82.212 028	4651	2.81	-0.43	-4.2	-10.5	1.015	44.85	72.87	12.39	-37.57	10.18	25.22	11.39	4.785	8.595	-0.729	0.731	0.191
12	J000347.2-475241	0.946 708	-47.877 917	4799	2.81	-0.60	28.2	14.6	0.785	-8.62	-100.97	8.18	14.86	7.61	-23.24	3.27	6.397	12.017	-1.035	1.036	0.322
13	J000347.5-832736	0.947 792	-83.459 861	4383	2.04	-0.51	-1.3	-3.4	1.343	-15.75	36.35	34.21	14.93	28.23	34.38	32.38	6.877	9.373	-1.053	1.049	0.062
14	J000401.7-211407	1.006 958	-21.235 167	4624	2.23	-0.57	-4.3	6.1	1.511	41.46	11.93	22.23	73.63	22.44	-23.53	4.90	7.955	15.539	-2.557	2.579	2.480
15	J000401.7-211407	1.006 958	-21.235 167	4763	2.62	-0.41	-4.3	6.1	1.511	42.90	12.09	22.23	73.69	22.44	-23.93	4.88	7.956	15.588	-2.588	2.602	2.858
16	J000405.7-454339	1.023 875	-45.727 583	4497	2.35	0.11	-6.0	-9.3	0.682	16.08	45.84	6.56	-6.79	6.69	4.27	2.61	6.569	8.910	-0.689	0.690	0.010
17	J000406.6-774539	1.027 417	-77.760 917	4886	2.83	-0.06	-0.4	6.4	1.438	-57.21	2.07	12.01	77.36	8.46	10.18	7.28	7.423	14.769	-1.495	1.494	2.074
18	J000431.7-412250	1.132 083	-41.380 556	4415	2.43	-0.13	6.6	-0.8	1.500	15.43	-20.36	14.44	-15.10	14.82	-15.32	4.53	6.944	8.011	-1.485	1.485	0.009
19	J000454.7-571529	1.228 042	-57.258 111	4760	2.60	-0.34	9.5	-18.7	1.739	44.73	24.17	20.72	-164.50	21.39	29.29	11.75	1.456	7.214	-3.777	1.918	999.999
20	J000509.7-503556	1.290 583	-50.598 889	4830	2.14	-0.80	-6.5	-2.1	2.091	95.62	119.22	21.64	-1.55	21.97	-60.53	9.73	5.674	11.893	-3.556	3.791	99.018
21	J000527.5-285808	1.447 875	-28.969 000	4760	2.35	-0.49	8.7	-12.7	0.863	17.41	3.22	7.85	-47.47	9.51	-15.60	1.50	5.286	7.886	-0.890	0.889	0.044
22	J000610.7-391521	1.544 458	-39.255 861	4965	2.69	-0.42	-0.2	-0.6	1.323	11.92	18.03	14.16	9.47	10.57	-3.96	3.37	7.564	8.994	-1.401	1.405	0.007
23	J000632.0-525213	1.633 292	-52.870 139	4558	2.10	-0.52	1.9	8.1	1.301	51.14	8.92	15.11	33.84	15.31	-62.00	7.34	7.654	11.065	-2.203	2.203	6.763
24	J000711.2-712952	1.796 500	-71.497 833	4890	2.72	-0.53	29.2	-9.1	1.420	4.98	-124.67	20.65	-122.94	18.60	11.35	15.22	2.414	9.459	-1.141	1.139	999.999
25	J000740.7-213330	1.919 500	-21.558 194	4727	2.05	-0.71	0.6	-4.0	0.738	39.03	14.19	8.44	7.53	8.56	-33.49	1.87	7.812	8.822	-0.986	0.983	0.034
26	J000740.7-213330	1.919 500	-21.558 194	4924	2.59	-0.47	0.6	-4.0	0.738	39.03	14.28	8.44	7.69	8.56	-34.43	1.79	7.814	8.841	-0.997	0.998	0.037
27	J000742.0-413624	1.924 833	-41.606 667	4889	2.52	-0.61	7.2	-0.9	1.294	-26.08	-29.22	11.91	-8.21	12.18	25.37	3.68	7.146	8.328	-1.432	1.434	0.018
28	J000743.4-200051	1.930 792	-20.014 083	4709	2.38	-0.15	15.1	-11.1	0.850	-10.49	-27.96	11.09	-54.84	11.51	0.76	2.49	4.860	8.074	-0.841	0.834	0.072
29	J000743.4-200051	1.930 792	-20.014 083	4575	2.24	-0.21	15.1	-11.1	0.850	-9.34	-27.86	11.09	-54.62	11.51	-0.36	2.60	4.872	8.075	-0.839	0.835	0.070
30	J000752.0-211211	1.966 458	-21.203 056	4554	2.17	-0.72	18.9	-30.2	0.812	-9.65	-3.35	10.53	-122.30	11.55	-8.88	2.34	2.298	7.926	-0.935	0.942	999.999
31	J000752.0-211211	1.966 458	-21.203 056	4747	2.50	-0.45	18.9	-30.2	0.812	-8.90	-3.28	10.53	-122.17	11.55	-9.61	2.43	3.203	7.927	-0.944	0.929	999.999
32	J000755.3-672223	1.980 417	-67.372 944	4642	2.46	-0.36	15.4	2.7	1.743	-42.89	-101.65	44.54	-8.32	42.07	3.60	31.86	5.927	10.986	-1.737	1.737	0.114
33	J000811.4-494952	2.047 417	-49.597 778	4551	2.59	-0.49	10.9	0.9	0.741	28.06	-4.72	5.94	-15.01	5.64	-23.78	4.05	6.900	7.739	-0.678	0.678	0.014
34	J000812.3-393058	2.051 042	-39.516 194	4966	2.58	-0.83	24.9	-8.0	1.278	-53.86	-111.17	15.03	-93.27	15.40	43.25	4.09	3.225	9.304	-1.881	1.882	999.999
35	J000815.0-404803	2.062 333	-40.800 944	4686	2.36	-0.76	10.0	-0.2	1.716	75.80	-36.38	39.42	-35.44	40.35	-79.37	11.47	6.205	8.411	-2.614	2.374	324.914
36	J000846.6-400516	2.194 083	-40.087 667	4857	2.88	-0.16	0.0	7.7	1.116	20.39	-0.06	15.92	46.96	16.33	-21.79	4.49	7.793	11.916	-1.527	1.530	0.102
37	J000910.9-392316	2.295 458	-39.387 722	4676	2.59	-0.42	9.3	-16.3	2.001	13.43	7.64	34.08	-165.20	35.34	10.55	9.18	1.694	7.425	-3.592	3.592	999.999
38	J000915.5-210409	2.314 500	-21.069 083	4659	2.89	-0.31	-14.0	-1.1	2.414	21.10	144.85	50.39	80.89	49.64	10.60	10.12	7.023	25.152	-5.456	6.218	999.999
39	J000942.1-565953	2.425 375	-56.997 917	4895	2.18	-0.70	15.1	3.0	0.939	1.69	-44.22	8.51	-7.76	8.30	-12.20	4.62	6.694	8.729	-0.884	0.883	0.012

low-probability thin-disc stars, respectively, whereas 646 and 1599 stars are low- and high-probability thick-disc stars (Table 1). The relative number of high-probability thick-disc (RC) stars is much larger than the corresponding ones in Coşkunoğlu et al. (2012) (2 per cent), i.e. 24 per cent.

4.2 Population classification using stellar vertical orbital shape

Both radial and vertical orbital eccentricities contain valuable information: here we consider the vertical orbit shape. Vertical orbital eccentricities were calculated, as described above, from numerically integrated orbits. We term this the dynamical method of population assignment, which complements the Bensby et al. (2003) approach. The distribution function of e_v is not consistent with a single Gaussian distribution, as is shown in Fig. 9. A two-Gaussian model however does provide an acceptable fit. For convenience, we separated our sample into three categories, i.e. stars with $e_v \leq 0.12$ (3448 stars), $0.12 < e_v \leq 0.25$ (2389 stars) and $e_v > 0.25$ (944 stars), and fitted their metallicities to their mean radial distances (R_m) in order to investigate the presence of a metallicity gradient for RAVE RC stars. We provide in Table 2 (see supporting information with the online version of the paper) for each star stellar parameters from the RAVE DR3, calculated kinematical and dynamical parameters and our stellar population assignment.

5 RESULTS

5.1 First hints of a metallicity gradient apparent in the RC sample of stars

We show in Fig. 10 the distribution of metallicities for our final sample of RAVE RC stars. The metallicity distribution for all populations is rather symmetric with a mode at $[M/H] \sim -0.4$ dex. In

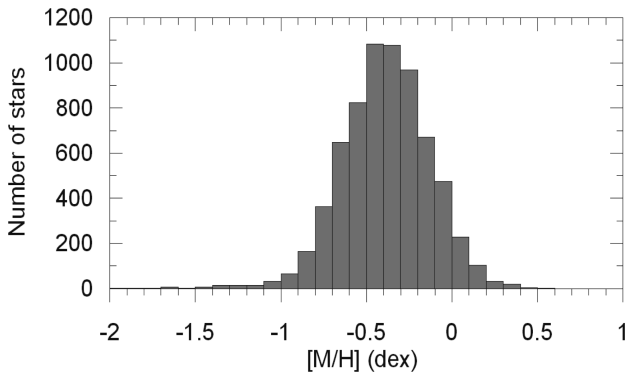


Figure 10. The metallicity distribution for our cleaned sample of RC stars, using RAVE DR3 abundances.

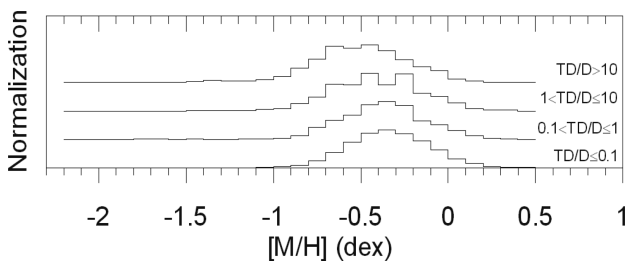


Figure 11. The normalized metallicity distribution as a function of assigned (probabilistic) population types.

Fig. 11 we show the normalized metallicity distribution functions, with the sample subdivided by probabilistic population assignment, as described above. This figure gives an indication of a systematic shift of the mode, shifting to low metallicities when one goes from the thin-disc stars to the thick-disc stars (Fig. 11). The z -distance distribution of our sample is shown in Fig. 12. While the typical star

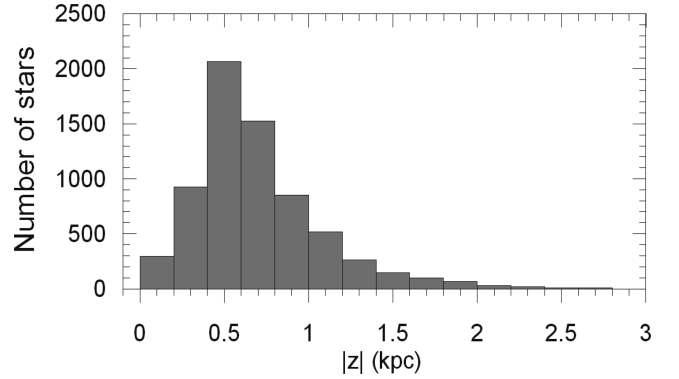


Figure 12. Distribution of the distances from the Galactic plane for our RC sample.

Table 3. The mean metallicity and vertical eccentricities as a function of the distance from the Galactic plane.

z ranges (kpc)	N	$\langle z \rangle$ (kpc)	$\langle [M/H] \rangle$ (dex)	$\langle e_v \rangle$
(0.0, 0.5]	2261	0.35	-0.33 ± 0.25	0.087 ± 0.106
(0.5, 1.0]	3376	0.70	-0.41 ± 0.25	0.161 ± 0.136
(1.0, 1.5]	857	1.19	-0.47 ± 0.25	0.271 ± 0.187
(1.5, 2.0]	222	1.71	-0.56 ± 0.25	0.378 ± 0.222
(2.0, 2.5]	54	2.20	-0.56 ± 0.24	0.460 ± 0.228

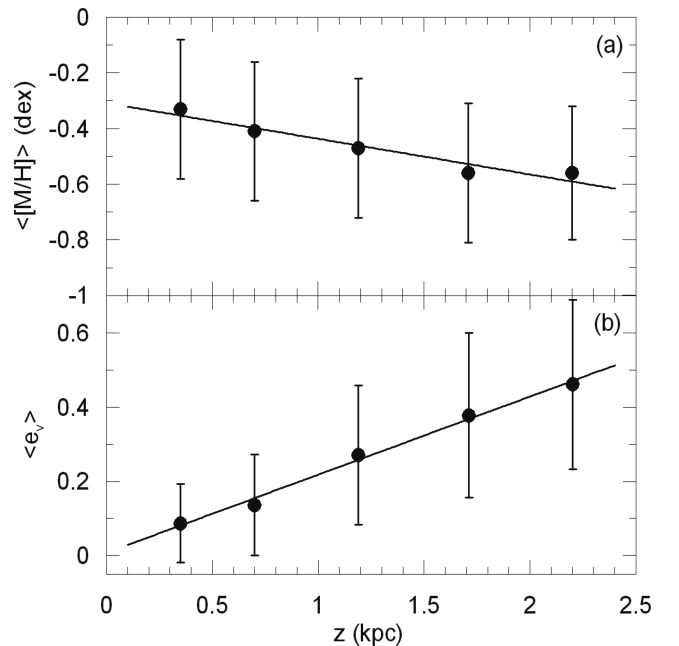


Figure 13. Variation of the mean metallicity (top) and vertical orbital eccentricity (bottom) as a function of the distance from the Galactic plane.

is at distance $|z| \sim 0.5$ kpc, there is a significant sample at larger distances. The range in z -distance is large enough to allow us to consider vertical metallicity gradient estimation.

The whole sample of stars, with no consideration of population assignment, were separated into five bins in distance, and mean

z -distances from the Galactic plane, mean metallicities and mean vertical eccentricities were calculated for each bin. These are presented in Table 3. Fig. 13 summarizes the dependence of the results on the vertical distance from the Galactic plane. The apparent variation of the mean metallicity with z -distance from the Galactic plane

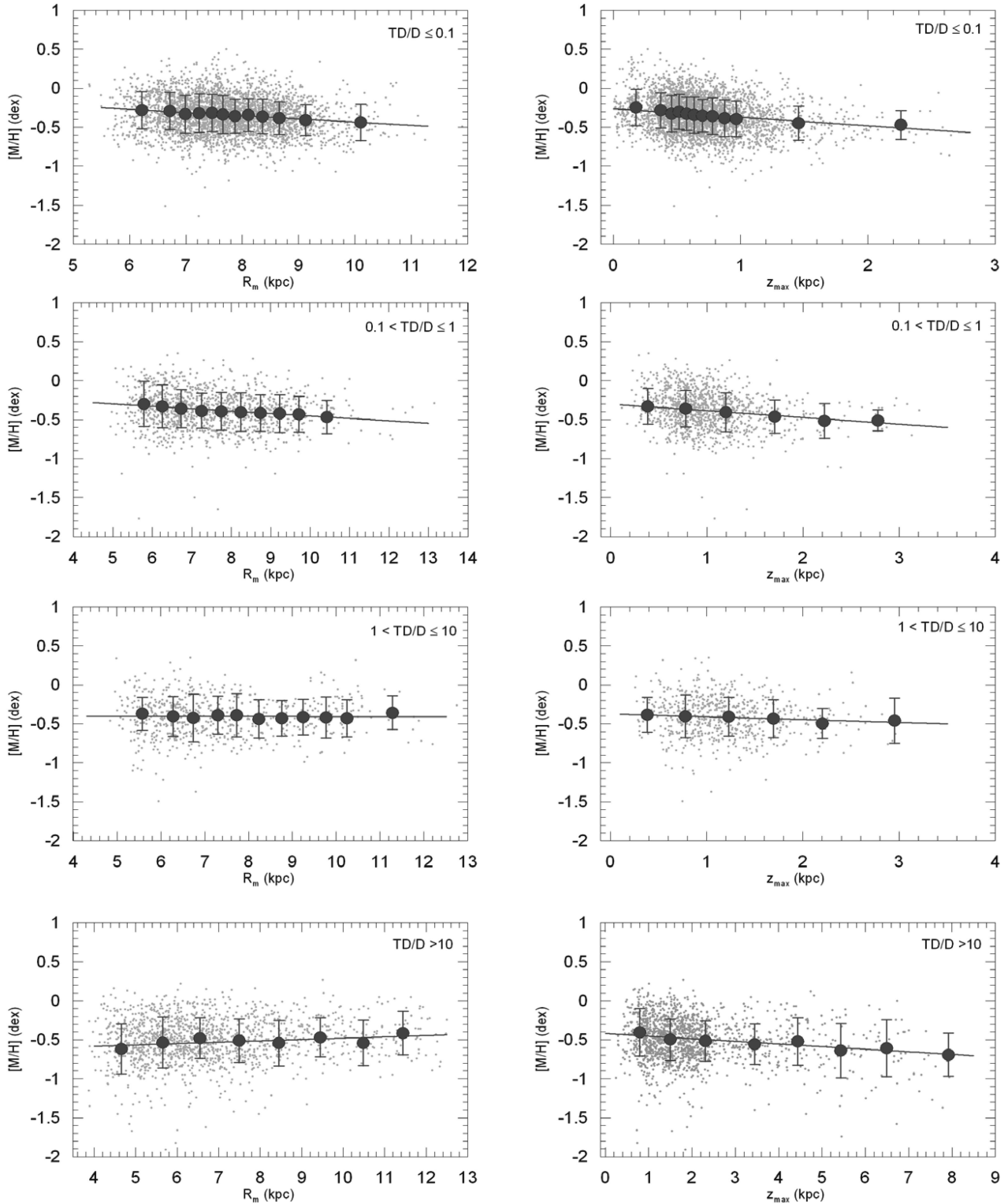


Figure 14. Radial (R_m -[M/H]) and vertical (z_{\max} -[M/H]) metallicity gradients for the RC subsamples, subdivided into probabilistic population types as described in the text.

in Fig. 13 indicates the existence of a vertical metallicity gradient for RC stars. This figure does not however allow discrimination between a true gradient in a consistently defined population (e.g. ‘thick disc’) and a changing relative contribution from two populations (e.g. ‘thin disc’ and ‘thick disc’), which have different modal abundances, and for which either one, both or neither has an intrinsic gradient. Also given in Fig. 13 is the variation of the vertical eccentricity with z , which again shows either a smooth transition from thin-disc to thick-disc eccentricities, or a changing population mix, or both discs.

5.2 Metallicity gradients using the kinematical population assignment method

We consider the metallicities as a function of the mean orbital Galactocentric radial distance (R_m) and maximum distance to the Galactic plane ($|z_{\max}|$) for each different population defined in Section 4, and test for the presence of vertical and radial metallicity gradients for each population. We fitted the distributions to linear equations, whose gradient is any metallicity gradient, $d[M/H]/dR_m$ or $d[M/H]/dz_{\max}$. The results are shown in Fig. 14.

The radial $d[M/H]/dR_m$ gradients are small or consistent with zero. The best determined value (largest ratio of the gradient value to the error value) is for low-probability thin-disc stars, where the gradient is $d[M/H]/dR_m = -0.031 \pm 0.003 \text{ dex kpc}^{-1}$ (Table 4). The only metallicity gradient consistent with zero (with small formal errors) is for low-probability thick-disc stars.

The vertical metallicity gradients are (absolutely) much larger than the radial ones, and are statistically detected. The largest gradient in the vertical direction is steeper for high-probability thin-disc stars, relative to the other populations, viz $d[M/H]/dz_{\max} = -0.109 \pm 0.008 \text{ dex kpc}^{-1}$. Additionally, the metallicity gradient for high-probability thick-disc stars is not zero, i.e. $d[M/H]/dz_{\max} = -0.034 \pm 0.003 \text{ dex kpc}^{-1}$.

5.3 Metallicity gradients using the dynamical population assignment method

We now consider the metallicities as a function of the mean orbital Galactocentric radial distance (R_m) and maximum distance to the Galactic plane ($|z_{\max}|$) for the populations defined by their eccentricities in Section 4.2, with one slight modification, in that we add a population defined by $e_v \leq 0.07$ (1269 stars) representing the blue stars. We make this modification due to our experience in analysing the RAVE dwarf stars. In Coşkunoğlu et al. (2012), we showed that the blue stars which have the smallest orbital eccentricities (most circular orbits) have also steeper metallicity gradients relative to samples with larger orbital eccentricities.

The results are presented in Table 4 and Fig. 15. The steepest metallicity gradient is for $e_v \leq 0.07$ in the vertical direction, i.e. $d[M/H]/dz_{\max} = -0.260 \pm 0.031 \text{ dex kpc}^{-1}$. The vertical metallicity gradient systematically decreases with increasing e_v values, becoming close to zero for the largest vertical eccentricities, $e_v > 0.25$. As noted above, our (RC giants) sample consists of thin- and thick-disc stars. The largest orbital eccentricities correspond to thick-disc stars.

That is, the vertical metallicity gradient for the thick disc is close to zero. The trend of the radial metallicity gradient is almost the same as the vertical metallicity gradient – less steep. For example, $d[M/H]/dR_m = -0.041 \pm 0.007 \text{ dex kpc}^{-1}$ for $e_v \leq 0.07$.

Table 4. Radial and vertical metallicity gradients for RC RAVE stars evaluated from kinematical and dynamical data. The meanings of the probabilistic population assignments, TD/D and e_v , are explained in the text.

Population type	$d[M/H]/dR_m$ (dex kpc $^{-1}$)	$d[M/H]/dz_{\max}$ (dex kpc $^{-1}$)	Sample size
$TD/D \leq 0.1$	-0.041 ± 0.003	-0.109 ± 0.008	3385
$0.1 < TD/D \leq 1$	-0.031 ± 0.003	-0.086 ± 0.013	1151
$1 < TD/D \leq 10$	-0.001 ± 0.005	-0.036 ± 0.016	646
$TD/D > 10$	0.017 ± 0.008	-0.034 ± 0.003	1599
$e_v \leq 0.07$	-0.041 ± 0.007	-0.260 ± 0.031	1269
$e_v \leq 0.12$	-0.025 ± 0.040	-0.167 ± 0.011	3448
$0.12 < e_v \leq 0.25$	-0.013 ± 0.004	-0.103 ± 0.008	2389
$e_v > 0.25$	0.022 ± 0.006	-0.022 ± 0.005	944

6 DISCUSSION AND CONCLUSION

We have used the RAVE DR3 to identify RC stars, further excluding cool stars, and those with the most uncertain space motions. We used the calibrated RAVE DR3 metallicities and the mean radial and maximum distances to investigate the presence of radial and vertical metallicity gradients, dividing the sample into a variety of subsamples.

We derive significant radial and vertical metallicity gradients for high-probability thin-disc stars and for the subsample with $e_v \leq 0.07$. We derive significant and marginally shallower gradients for the other subsamples. We do not detect any significant gradients for thick-disc stars. Vertical metallicity gradients are much steeper than the radial ones, for the same subsample, as (perhaps) expected. We derive the metallicity gradients for the subsample with $e_v \leq 0.07$, which are the youngest sample stars, to be $d[M/H]/dR_m = -0.041 \pm 0.007$ and $d[M/H]/dz_{\max} = -0.260 \pm 0.031 \text{ dex kpc}^{-1}$.

The radial metallicity gradients for all subsamples are rather close to the corresponding ones obtained for F-type dwarfs. Hence, the discussion in Coşkunoğlu et al. (2012) is also valid here. We cannot determine any vertical metallicity gradient for RAVE dwarfs due to their small distances from the Galactic plane. However, we can compare our results with those obtained for giants. Chen et al. (2011) investigated the metallicity gradient of the thick disc by using RHB stars from SDSS DR8 (Aihara et al. 2011) and they found two different vertical metallicity gradients estimated in two ways. One is a fit to the Gaussian peaks of the metallicity histograms of the thick disc by subtracting minor contributions from the thin disc and the inner halo based on the Besançon Galaxy model (Robin et al. 1996). The resulting gradient is $d[M/H]/dz = -0.12 \pm 0.01 \text{ dex kpc}^{-1}$ for $0.5 < |z| < 3 \text{ kpc}$. The other method is fitting the data linearly for the stars ($1 < |z| < 3 \text{ kpc}$) where the thick disc is the dominant population. Five subgroups were then selected in different directions in the $X-|z|$ plane to investigate the difference in the vertical metallicity gradient between the Galactocentric and anti-Galactocentric directions. They found that a vertical gradient of $d[M/H]/dz = -0.22 \pm 0.07 \text{ dex kpc}^{-1}$ was detected for five directions except for one involving the population of stars from the bulge.

Neither of the vertical metallicity gradients claimed by Chen et al. (2011) are in agreement with our results, nor are they consistent with studies appearing in previous works in the literature.

Another recent investigation of the vertical metallicity gradient for the thick disc is that of Ruchti et al. (2011). In that paper the authors gave a sample of 214 red giant branch stars, 31 RC/RHB

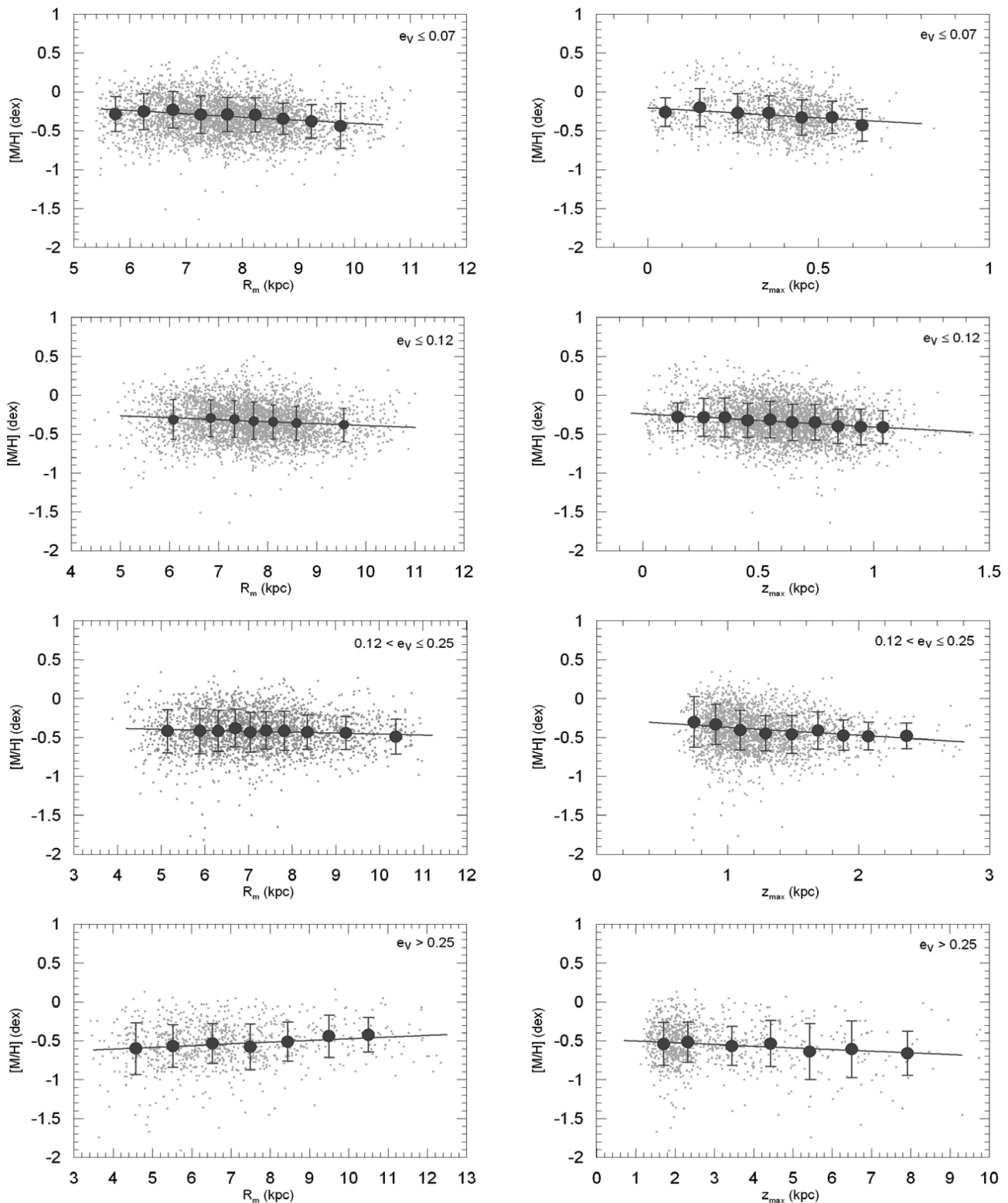


Figure 15. Radial (R_m -[M/H]) and vertical (z_{\max} -[M/H]) metallicity gradients for the RC subsamples, subdivided by vertical orbital eccentricity.

stars and 74 main-sequence/subgiant branch metal-poor stars. They found that the thick disc $[\alpha/\text{Fe}]$ ratios are enhanced and have little variation (<0.1 dex). Their sample further allowed, for the first time, investigation of the gradients in the metal-poor thick disc. For stars with $[\text{Fe}/\text{H}] < -1.2$ dex, the thick disc shows very small

gradients, $<0.03 \pm 0.02$ dex kpc^{-1} , in α enhancement, while they found a $d[\text{Fe}/\text{H}]/dR = +0.01 \pm 0.04$ dex kpc^{-1} radial gradient and a $d[\text{Fe}/\text{H}]/dz = -0.09 \pm 0.05$ dex kpc^{-1} vertical gradient in iron abundance. We consider only the gradient in iron abundance, not the gradient in α enhancement. We may transform published iron

abundances to RAVE metallicity values by means of the equation (Zwitter et al. 2008)

$$[M/H] = [Fe/H] + 0.11[1 \pm (1 - e^{-3.6[Fe/H]+0.55})]. \quad (10)$$

This reveals that the Ruchti et al. (2011) vertical gradient is consistent with the vertical metallicity gradient determined here, within the errors, for high-probability thick-disc stars, $d[Fe/H]/dz_{\max} = -0.034 \pm 0.003 \text{ dex kpc}^{-1}$. However, there is a difference between the corresponding radial metallicity gradients in the two studies. An explanation for this disagreement may be the differing metallicity range of the sample stars used in the two works. In the present study we consider stars with $[M/H] > -1.1$ dex, with a minority at the metal-poor tail in our work, while the corresponding selection is $[Fe/H] < -1.2$ dex in Ruchti et al. (2011).

The radial metallicity gradients we have estimated from RC giant stars are consistent with those derived in paper II for dwarfs (Coşkunoğlu et al. 2012). The robust metallicity gradients we determine are $d[M/H]/dR_m = -0.041 \pm 0.003 \text{ dex kpc}^{-1}$ for the high-probability thin-disc stars, the population type labelled with $TD/D \leq 0.1$, and $d[M/H]/dR_m = -0.041 \pm 0.07 \text{ dex kpc}^{-1}$ for the sample with eccentricity $e_v \leq 0.07$. Samples biased to low-probability thin-disc and thick-disc stars show systematically shallower gradients. Complementary to the dwarf sample, the distance range of the RC giant stars, with a median distance of 1.4 kpc, provides information on vertical metallicity gradients. The vertical metallicity gradients for the high-probability thin-disc stars and for the sample with $e_v \leq 0.07$ are $d[M/H]/dz_{\max} = -0.109 \pm 0.008$ and $d[M/H]/dz_{\max} = -0.260 \pm 0.031 \text{ dex kpc}^{-1}$, respectively. For high-probability thick-disc stars we could detect a vertical metallicity gradient – a shallow one however, i.e. $d[M/H]/dz_{\max} = -0.034 \pm 0.003 \text{ dex kpc}^{-1}$.

From our analysis, we may conclude that, despite their greater distances from the Galactic plane, the RAVE DR3 RC giant stars confirm the radial metallicity gradients found for RAVE DR3 dwarf stars. Because of their greater distances from the Galactic plane, the RAVE DR3 RC stars also permit vertical metallicity gradients to be measured. These findings can be used to constrain formation scenarios of the thick and thin discs.

ACKNOWLEDGMENTS

We would like to thank the referee Dr Martin López-Corredoira for his useful suggestions that improved the readability of this paper.

Funding for RAVE has been provided by the Australian Astrophysical Observatory; the Leibniz-Institut fuer Astrophysik Potsdam (AIP); the Australian National University; the Australian Research Council; the French National Research Agency; the German Research Foundation; the European Research Council (ERC-StG 240271 Galactica); the Istituto Nazionale di Astrofisica at Padova; The Johns Hopkins University; the National Science Foundation of the USA (AST-0908326); the W. M. Keck foundation; the Macquarie University; the Netherlands Research School for Astronomy; the Natural Sciences and Engineering Research Council of Canada; the Slovenian Research Agency; the Swiss National Science Foundation; the Science & Technology Facilities Council of the UK; Opticon; Strasbourg Observatory and the Universities of Groningen, Heidelberg and Sydney. The RAVE web site is at <http://www.rave-survey.org>

This publication makes use of data products from the Two Micron All Sky Survey, which is a joint project of the University of Massachusetts and the Infrared Processing and Analysis

Center/California Institute of Technology, funded by the National Aeronautics and Space Administration and the National Science Foundation. This research has made use of the SIMBAD, NASA's Astrophysics Data System Bibliographic Services and the NASA/IPAC ExtraGalactic Database (NED) which is operated by the Jet Propulsion Laboratory, California Institute of Technology, under contract with the National Aeronautics and Space Administration.

REFERENCES

- Abazajian K. et al., 2003, AJ, 126, 2081
 Aihara H. et al., 2011, ApJS, 193, 29
 Ak S., Bilir S., Karaali S., Buser R., 2007a, Astron. Nachrichten, 328, 169
 Ak S., Bilir S., Karaali S., Buser R., Cabrera-Lavers A., 2007b, New Astron., 12, 605
 Alves D. R., 2000, ApJ, 539, 732
 Bensby T., Feltzing S., Lundström I., 2003, A&A, 410, 527
 Bensby T., Feltzing S., Lundström I., Ilyin I., 2005, A&A, 433, 185
 Bilir S., Karaali S., Ak S., Yaz E., Hamzaoglu E., 2006, New Astron., 12, 234
 Bilir S., Cabrera-Lavers A., Karaali S., Ak S., Yaz E., López-Corredoira M., 2008, PASA, 25, 69
 Bilir S., Karaali S., Ak S., Önal Ö., Coşkunoğlu B., Seabroke G. M., 2011, MNRAS, 418, 444
 Buser R., Rong J., Karaali S., 1999, A&A, 348, 98
 Cabrera-Lavers A., Bilir S., Ak S., Yaz E., López-Corredoira M., 2007, A&A, 464, 565
 Chen Y. Q., Zhao G., Carrell K., Zhao J. K., 2011, AJ, 142, 184
 Coşkunoğlu B. et al., 2011, MNRAS, 412, 1237
 Coşkunoğlu B., Ak S., Bilir S., Karaali S., Önal Ö., Yaz E., Gilmore G., Seabroke G. M., 2012, MNRAS, 419, 2844
 Cutri R. M. et al., 2003, The IRSA 2MASS All-Sky Point Source Catalog, NASA/IPAC Infrared Science Archive (<http://irsa.ipac.caltech.edu/applications/Gator/>)
 Dehnen W., 1998, AJ, 115, 2384
 De Simone R. S., Wu X., Tremaine S., 2004, MNRAS, 350, 627
 Dinescu D. I., Girard T. M., van Altena W. F., 1999, AJ, 117, 1792
 Du C., Zhou X., Ma J., Shi J., Chen A. B., Jiang Z., Chen J., 2004, AJ, 128, 2265
 ESA, 1997, ESA SP-1200, The Hipparcos and Tycho Catalogues. ESA, Noordwijk
 Famaey B. et al., 2005, A&A, 430, 165
 Famaey B., Siebert A., Jorissen A., 2008, A&A, 483, 453
 Fiorucci M., Munari U., 2003, A&A, 401, 781
 Groenewegen M. A. T., 2008, A&A, 488, 25
 Hernquist L., 1990, ApJ, 356, 359
 Johnson D. R. H., Soderblom D. R., 1987, AJ, 93, 864
 Johnston K. V., Spergel D. N., Hernquist L., 1995, ApJ, 451, 598
 Karaali S., Bilir S., Karataş Y., Ak S. G., 2003, PASA, 20, 165
 Keenan P. C., Barnbaum C., 1999, ApJ, 518, 859
 Luck R. E., Lambert D. L., 2011, AJ, 142, 136
 Luck R. E., Kovtyukh V. V., Andrievsky S. M., 2006, AJ, 132, 902
 Luck R. E., Andrievsky S. M., Kovtyukh V. V., Gieren W., Graczyk D., 2011, AJ, 142, 51
 Mihalas D., Binney J., 1981, Galactic Astronomy: Structure and Kinematics, 2nd edn. Freeman & Co., San Francisco
 Miyamoto M., Nagai R., 1975, PASJ, 27, 533
 Nordström B. et al., 2004, A&A, 418, 989
 Paczynski B., Stanek K. Z., 1998, ApJ, 494, L219
 Pauli E. M., 2005, in Gerdjikov V., Tsvetkov M., eds, Prof. G. Manev's Legacy in Contemporary Astronomy, Theoretical and Gravitational Physics. Heron Press Limited, Sofia, Bulgaria, p. 185
 Peng X., Du C., Wu Z., 2011, preprint (arXiv:1111.4719)
 Pompéia L. et al., 2011, MNRAS, 415, 1138

- Puzeras E., Tautvaišienė G., Cohen J. G., Gray D. F., Adelman S. J., Ilyin I., Chorniy Y., 2010, *MNRAS*, 408, 1225
- Robin A. C., Haywood M., Créze M., Ojha D. K., Bienaymé O., 1996, *A&A*, 305, 125
- Roeser S., Demleitner M., Schilbach E., 2010, *AJ*, 139, 2440
- Rong J., Buser R., Karaali S., 2001, *A&A*, 365, 431
- Ruchti G. R. et al., 2011, *ApJ*, 737, 9
- Shaver P. A., McGee R. X., Newton L. M., Danks A. C., Pottasch S. R., 1983, *MNRAS*, 204, 53
- Siebert A. et al., 2011, *AJ*, 141, 187
- Skrutskie M. F. et al., 2006, *AJ*, 131, 1163
- Skuljan J., Hearnshaw J. B., Cottrell P. L., 1999, *MNRAS*, 308, 731
- Steinmetz M. et al., 2006, *AJ*, 132, 1645
- Trefzger C. F., Pel J. W., Gabi S., 1995, *A&A*, 304, 381
- van Leeuwen F., 2007, *A&A*, 474, 653
- Wilson M. L. et al., 2011, *MNRAS*, 413, 2235
- Yaz E., Karaali S., 2010, *New Astron.*, 15, 234
- Zwitter T. et al., 2008, *AJ*, 136, 421

SUPPORTING INFORMATION

Additional Supporting Information may be found in the online version of this paper.

Table 2. Stellar atmospheric parameters, astrometric, kinematic and dynamic data for the whole sample.

Please note: Wiley-Blackwell are not responsible for the content or functionality of any supporting materials supplied by the authors. Any queries (other than missing material) should be directed to the corresponding author for the paper.

This paper has been typeset from a $\text{\TeX}/\text{\LaTeX}$ file prepared by the author.